



Draft genome sequence of endophytic fungus *Fusarium proliferatum* ZO-L2-4 and analysis of its secondary metabolite biosynthetic potential

Ni Putu Ariantari^{1*}, I Putu Yogi Astara Putra¹, I Putu Prakasa Wiprayoga², Andri Frediansyah³, Ni Wayan Prasanthi Swarna Putri¹, Anak Agung Istri Padma Suari¹, Komang Tria Noviana Dewi¹, Ketut Widyani Astuti¹, Made Pharmawati⁴

¹Department of Pharmacy, Faculty of Mathematics and Natural Sciences, Udayana University, Badung, Indonesia.

²Faculty of Science, The University of Melbourne, Parkville, Australia.

³Research Center for Food Technology and Processing, National Research and Innovation Agency (BRIN), Gunungkidul, Indonesia.

⁴Biology Study Program, Faculty of Mathematics and Natural Sciences, Udayana University, Badung, Indonesia.

ARTICLE HISTORY

Received on: 26/09/2025

Accepted on: 23/01/2026

Available Online: 05/03/2026

Key words:

Biosynthetic gene clusters, endophytic fungus, *Fusarium proliferatum* ZO-L2-4, polyketide synthases, nonribosomal peptide synthase.

ABSTRACT

Fusarium proliferatum has been widely reported as a promising producer of bioactive secondary metabolites. In this study, we conducted genome mining to investigate the putative biosynthetic gene clusters (BGCs) from the fungal strain *F. proliferatum* ZO-L2-4 isolated from the leaves of *Zingiber officinale* Roscoe (ginger). First, the fungal gDNA was extracted and then subjected to library preparation. Next, it was sequenced using Illumina NextSeq 2000. The contigs were assembled, then the genes were predicted using AUGUSTUS and GeneMark and annotated using Kyoto Encyclopedia of Genes and Genomes. The BGCs analysis was conducted using Antibiotics and Secondary Metabolites Analysis Shell (AntiSMASH) Fungal Version. From sequencing and assembly, we obtained a genome sequence in a size of 43.6 Mb consisting of 12 nuclear and one mitochondrial contigs, N50 of 4,304,280 bp, L50 of 5, and GC content of 48.14%. Genome annotation suggested that the predicted genes mainly functioned in global maps, followed by carbohydrate metabolism and amino acid metabolism. The AntiSMASH analysis identified 43 BGCs, dominated by terpene biosynthetic genes, nonribosomal peptide synthase (NRPS), NRPS-like, polyketide synthases, and hybrids. Among these, only six BGCs showed the highest homology with the gene clusters that are responsible for the biosynthesis of oxyjavanicin, choline, bikaverin, *Alternaria citri* toxin (ACT)-toxin II, koraiol, and gibepyrone-A. Most of the remaining were unknown by far. Putative identification employing high-resolution mass spectrometry suggested the presence of beauvericin as the predominant metabolite, along with tryptophol, terpestacin, ergosterol peroxide, indole, and terpendole E in the methanolic extract of *F. proliferatum*. These findings enhance our understanding of the molecular biology of the *Fusarium* genus and may pave the way for discovering novel bioactive secondary metabolites from this fungal strain through gene knockout and heterologous expression.

1. INTRODUCTION

The growing interest in endophytic fungi as a source of bioactive compounds has driven research into their genetic

and biosynthetic potential [1,2]. Endophytic fungi are fungi that reside inside the healthy plant tissues without causing apparent harm to their host. These fungi are involved in producing secondary metabolites that can benefit their host plants by promoting growth [3], providing stress tolerance [4], or offering protection against pathogens [5]. Additionally, the unique biochemical machinery of endophytic fungi has attracted attention for its potential to yield novel pharmaceuticals or other relevant compounds [6,7].

*Corresponding Author

Ni Putu Ariantari, Department of Pharmacy, Faculty of Mathematics and Natural Sciences, Udayana University, Badung, Indonesia.

E-mail: putu_ariantari@unud.ac.id

Fungi from the genus *Fusarium* are widely distributed in nature and are known for their capability to produce various bioactive compounds [8–10]. *Fusarium proliferatum*, a ubiquitous endophytic fungus, has been reported in diverse ecological niches, including association with medicinal plants such as ginger (*Zingiber officinale* Roscoe) [11]. Ginger is widely known for its traditional medicinal applications [12,13]. The use of ginger has shown potential in reducing nausea and vomiting due to chemotherapy in pediatric patients [14]. In addition, active compounds such as gingerol and shogaol are known to have strong antioxidant activity as well as their potential as anti-inflammatory agents [15]. Interestingly, these two compounds also show potential in addressing age-related neurological disorders [16]. In addition, ginger also serves as a reservoir for a diverse microbiome that may contribute to its bioactivity [17,18]. Among its microbial symbionts, *F. proliferatum* is of particular interest due to its ability to produce a variety of secondary metabolites with various bioactive potency, including antimicrobial and anticancer activities [19,20].

Our previous study has screened the bioactivity of the methanolic extract of *F. proliferatum* ZO-L2-4 isolated from the leaves of ginger. From the liquid chromatography-tandem mass spectrometry (LC-MS/MS) analysis, we tentatively identify one of the metabolites in this extract as 8-*O*-methylbostrycoidin [11]. Despite its antimicrobial and cytotoxic potential found in the previous study, the biosynthetic capabilities of this fungal strain remain underexplored, prompting genomic studies to uncover its hidden metabolic potential.

Genome sequencing and analysis provide a comprehensive platform to unearth the biosynthetic gene clusters (BGCs) responsible for secondary metabolite production in microbes, including fungi [21]. Advances in next-generation sequencing technologies and bioinformatics tools have enabled the identification and annotation of BGCs, which offer insights into the genetic basis of metabolite biosynthesis [22]. Such studies not only enlighten the metabolic potential of fungi but also facilitate the discovery of novel bioactive compounds [23].

In this study, we report the draft genome sequence of the endophytic fungus *F. proliferatum* ZO-L2-4, isolated from ginger. This work aims to elucidate the genetic framework underlying its secondary metabolite biosynthesis, providing a foundation for future investigations into its biotechnological applications. By analysing the genome for BGCs, we seek to uncover the metabolic potential of *F. proliferatum* ZO-L2-4.

2. MATERIALS AND METHODS

2.1. Fungal material

The fungal isolate *F. proliferatum* ZO-L2-4 was obtained from the leaves of *Z. officinale* in our previous study [11]. The fungal isolate was grown on agar media consisting of Bacto agar, yeast extract, malt extract, glycerol, and demineralized water for 3 days at room temperature.

2.2. Procedure

2.2.1. Genome extraction

High molecular weight gDNA was extracted using Quick-DNA Magbead Plus Kit (ZymoResearch, D4082).

2.2.2. Library preparation and genome sequencing

Total gDNA was used for the input of the library preparation. It was prepared using xGen DNA Library Prep EZ UNI Kit (IDT, 10009822). The gDNA was fragmented using enzymatic methods to match the expected insert size. The fragmented DNA was ligated with Illumina-compatible Adapter with unique index for each sample (Forward adapter: CAAGCAGAAGACGGCATACGAGAT[i7]GTCTCGTGGGCTCGG; reverse adapter: AATGATACGGCGACCACCGAGATCTACAC[i5]TCGTCGGCAGCGTC). The PCR was conducted to amplify the library. *Fusarium proliferatum* (GCA_036288945.1) was used as the reference for genome assembly. The quality and quantity of library samples were determined using Tape Station and Qubit Fluorometer, respectively. Sequencing was conducted using the Illumina NextSeq 2000 platform with 300-cycle paired-end (PE150) short reads.

2.2.3. Genome assembly and annotation

Data filtering was conducted using fastp, and the filtered reads were processed for variant calling using the GATK pipeline. Read quality was assessed with FastQC and summarized with MultiQC. Data transformation was carried out with Samtools, and variant calling was performed using GATK4. Variants were filtered, and a consensus sequence was generated using Bcftools. Variant annotation was completed with SnpEff. The quality of the assembled sequence was determined using Quast and Qualimap. Genome completeness was evaluated using Benchmarking Universal Single-Copy Orthologs (BUSCOs). Gene prediction was performed using AUGUSTUS and GeneMark for evidence-based gene model prediction. The predictions generated by BRAKER were used as the gene models for downstream analyses. Predicted coding sequences were subsequently annotated using evolutionary genealogy of genes: Non-supervised Orthologous Groups (eggNOG-mapper) for orthology-based functional assignment, including Pfam domain identification, Kyoto Encyclopedia of Genes and Genomes (KEGG) pathway mapping, and Clusters of Orthologous Genes (COG) category classification.

2.2.4. Core and accessory chromosome assessment

To characterize putative accessory chromosomes, each assembled scaffold was analyzed for genomic features, including Guanine-Cytosine (GC) content, repeat content, and gene content. GC content was calculated using Quast. Transposable element content was assessed by calculating the percentage of masked bases identified by RepeatMasker with both Dfam and custom RepeatModeler libraries trained on the reference genome *F. proliferatum* (GCA_036288945.1). The presence of conserved single-copy orthologs was assessed using BUSCO. Scaffolds with high repeat content, reduced BUSCO gene representation, and deviating GC content were considered as putative accessory chromosomes.

2.2.5. BGCs analysis

BGCs analysis was performed using Antibiotics and Secondary Metabolites Analysis Shell (AntiSMASH) Fungal Version. Visualization was done using Circos.

2.2.6. Fungal fermentation and extraction

Fungal endophyte *F. proliferatum* ZO-L2-4 was fermented on two Erlenmeyer flasks (1l) of sterile rice media containing 100 g of rice and 110 ml of distilled water, following the procedure described before [11]. Extraction of metabolite was done by adding 500 ml of ethyl acetate (EtOAc) into each flask at the end of rice fermentation, followed by solvent removal using a vacuum rotary evaporator, yielding 2.3 g crude EtOAc extract. The crude extract was then subjected to liquid-liquid partitioning between aqueous methanol and *n*-hexane to obtain the methanolic extract (795.5 mg) and *n*-hexane extract (1.5 g). The methanolic extract was used for high-resolution mass spectrometry (HRMS) analysis.

2.2.7. HRMS analysis

For HRMS analysis, the methanolic extract (50 mg) was dissolved in Mass Spectrometry (MS) grade methanol (1 ml). For the spectrometric analysis, a Q Exactive™ high resolution accurate mass LC-MS/MS system (Thermo Scientific™) was employed, coupled with a Thermo Scientific™ Vanquish™ Flex Ultra-High Performance Liquid Chromatography (UHPLC) setup. The Liquid Chromatography (LC) method utilized a flow rate of 0.3 ml/min and a 3 µl injection volume, with the mobile phase composed of 0.1% formic acid in H₂O (solvent A) and 0.1% formic acid in acetonitrile (solvent B). The gradient program started with 5% solvent B, ramping to 90% over 16 minutes, followed by an isocratic hold at 90% B for 4 minutes, and a final gradient returning to 5% B over 5 minutes. Chromatographic separation was achieved using a 2.6 µm Accucore™ Phenyl Hexyl 100 × 2 mm column. The mass spectrometer was operated within the *m/z* range of 150 to 1,800 for MS scans. Instrumental settings included a sheath gas flow of 15, an auxiliary gas flow of 5, a spray voltage of 3.6 kV, and a capillary temperature of 32 °C. The auxiliary gas heater temperature was maintained at 3 °C, and the S-lens Radio Frequency (RF) level was set to 50. The MS resolution was adjusted to 70,000 with an automatic gain control (AGC) target of 3e⁶ and a maximum injection time (IT) of 250 ms. For the dd-MS² scans, the resolution was set to 17,500, the AGC target to 1e⁵, and the maximum IT to 60 ms. The number of loop counts was set to 5, with collision energies of 18, 35, and 53. TopN and isolation window values were set to 5 and 1.0 *m/z*, respectively. The minimum AGC target for data-dependent acquisition was 9e³, with an intensity threshold of 1.3e⁵, and charge exclusion was applied for ions with charges of 4–8 and >8. Isotope exclusion was enabled, with dynamic exclusion time set to 10 seconds. Caffeine served as the calibration standard in this study. Chromatogram and metabolomic data analysis were performed using Compound Discoverer 3.2 (Thermo Scientific™), interfacing with mzCloud (www.mzcloud.org) and ChemSpider (www.chemspider.com), along with publicly available databases from the Global Natural Products Social Molecular Networking (GNPS) (https://gnps.ucsd.edu).

3. RESULTS AND DISCUSSION

3.1. Genome sequencing and assembly

From sequencing of *F. proliferatum* ZO-L2-4 (Fig. 1), we generated 35.2 million raw reads comprising 5.3 Gbp nucleotides, which were filtered, resulting in a final dataset of 34.6

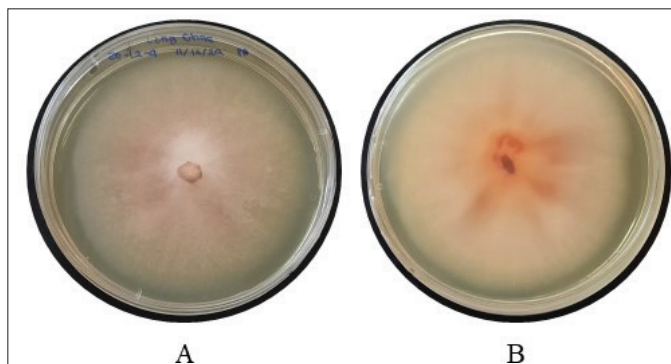


Figure 1. The morphological appearance of *F. proliferatum* ZO-L2-4 grown on media containing Bacto agar, yeast extract, malt extract, glycerol, and demineralized water, (A) top and (B) bottom of agar media.

Table 1. Assembly statistics of *F. proliferatum* ZO-L2-4.

Item	Value
Before filtering	
Total reads	35.221294 M
Total bases	5.318415 G
Q20 bases	97.357389 %
Q30 bases	93.809545%
GC content	48.298102%
After Filtering	
Total reads	34.580216 M
Total bases	4.954088 G
Q20 bases	98.257572%
Q30 bases	95.064806%
GC content	48.141149%
Genome size	43,628,202
Coverage	88.45 %
Contigs	13
Largest contig (bp)	6,173,545 bp
N50	4,304,280 bp
N90	2,463,860 bp
L50	5
L90	10
BUSCO (C)	97.6%
BUSCO (S)	97.5%
BUSCO (D)	0.1%
BUSCO (F)	0.3%
BUSCO (M)	2.1%

million reads totaling 4.9 Gbp nucleotides (Table 1). Although this process reduced the amount of sequence data, the Q30 value improved, increasing from 93.8% to 95.1%. The filtered reads were assembled into the complete genome of *F. proliferatum* ZO-L2-4, yielding a total genome size of 43.63 Mbp comprised of 12 nuclear and one mitochondrial contigs, with the largest contig has size of 6.17 Mbp. It showed N50 of 4,304,280 bp, L50 of 5,

and GC content of 48.14%. The results indicated that genome assembly was of high quality. Genome assembly also showed a BUSCO completeness score of 97.6% (88.45% coverage), suggesting that we obtained a highly contiguous and complete genome. The draft genome from this strain has been submitted to NCBI GenBank under BioSample accession of SAMN45994223 and BioProject ID of PRJNA1203388.

3.2. Genome annotation

From gene prediction using AUGUSTUS, we found that 11,308 genes (8.0%) and 35,654 protein coding sequences (CDSs) (25.3%), while from analysis using GeneMark, it showed 1,039 genes (1.5%), 5,472 mRNAs (8%), and 1,6791 CDSes (24.7%). As shown in Figure 2, gene annotation against KEGG database revealed that those genes were classified into metabolism (40.6%), human diseases (20.7%), genetic information processing (11.6%), organismal systems (11.1%), cellular processes (10.0%), and environmental information (6.0%). In metabolism class, most of the genes are involved in the function of global maps (1,792),

followed by carbohydrate metabolism (316), and amino acid metabolism (310). The annotation data were published in Zenodo (<https://doi.org/10.5281/zenodo.15833454>)

3.3. Functional annotation and orthology assignment

Gene models predicted by BRAKER were further annotated to provide orthology-based validation. Out of 16,801 predicted coding sequences, 98.5% were assigned to orthologous groups, 79.3% were assigned a functional description, and 78.1% contained at least one Pfam domain. KEGG annotation was identified for 34.9% of CDSes, while 79.3% were classified into COG functional categories. These results indicate a high proportion of protein-coding genes with conserved domains and known orthologs, supporting the completeness and reliability of the gene prediction (Table 2).

3.4. Core and accessory chromosome assessment

To distinguish core from putative accessory chromosomes, we examined GC content, BUSCO gene count,

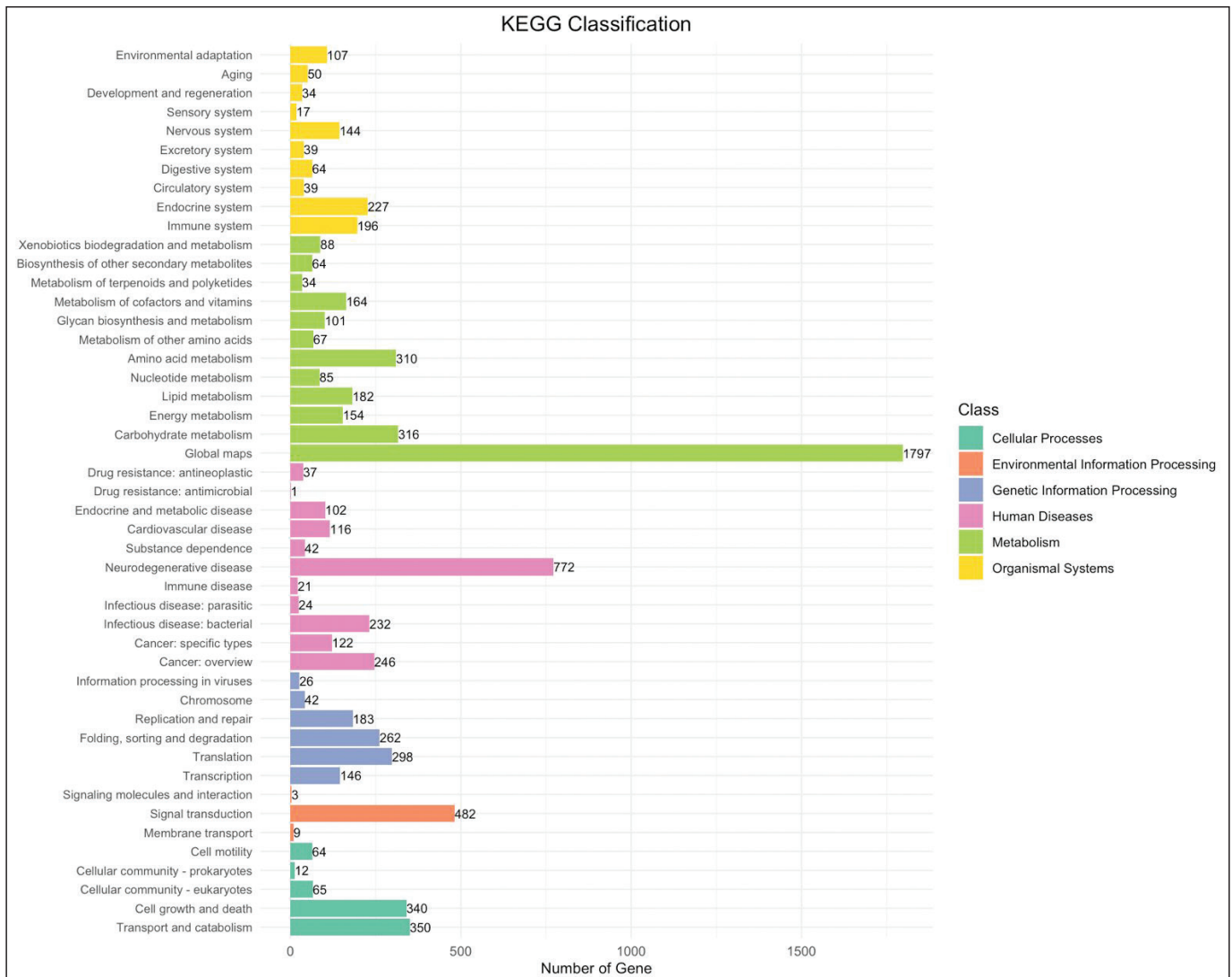


Figure 2. Functional annotation of the genes from *F. proliferatum* ZO-L2-4 according to the KEGG database.

Table 2. Functional annotation summary of predicted CDS.

Feature	*Percentage (%)
CDS assigned to orthologous groups	98.5
CDS assigned functional descriptions	79.3
CDS containing at least one Pfam domain	78.1
CDS with KEGG annotations	34.9
CDS classified into COG categories	79.3

*Percentages are relative to 16,801 predicted CDS.

Table 3. Summary of contig features used to identify putative accessory chromosomes.

*Contig	GC content (%)	BUSCO gene count	Interspersed repeats (%)
ZO-L2-4_1	0.49	906	0.80
ZO-L2-4_2	0.49	637	1.35
ZO-L2-4_3	0.49	655	0.88
ZO-L2-4_4	0.49	395	0.76
ZO-L2-4_5	0.49	552	0.95
ZO-L2-4_6	0.49	427	1.14
ZO-L2-4_7	0.49	413	1.33
ZO-L2-4_8	0.49	153	1.48
ZO-L2-4_9	0.49	251	1.24
ZO-L2-4_10	0.49	5	1.23
ZO-L2-4_11	0.49	7	1.43
ZO-L2-4_12	0.48	0	4.40

*Contig ZO-L2-4_13, representing the mitochondrial chromosome, was not included in this summary.

and interspersed repeat content across all contigs (Table 3). Most contigs showed relatively uniform GC content (approximately 49%) and high BUSCO gene counts, typical of conserved core chromosomes. In contrast, several contigs, particularly ZO-L2-4_12, ZO-L2-4_10, and ZO-L2-4_11, showed markedly reduced BUSCO counts (zero or near zero). Specifically, ZO-L2-4_12 showed significantly elevated interspersed repeat percentages (4.40%). These patterns are characteristic of accessory chromosomes, which frequently display lower conserved gene density and increased repeat accumulation relative to the core genome. Collectively, these results suggest the presence of accessory genomic regions within the assembly, particularly in the contig ZO-L2-4_12. This contig does not appear to contain BGC.

Contig ZO-L2-4_12 exhibited two notable genomic features: a high proportion of repetitive sequences and the complete absence of BUSCO genes. These characteristics are consistent with previously described accessory chromosomes, which are dispensable for viability but may contribute to adaptive traits such as host-pathogen interaction [24]. To evaluate the potential involvement of ZO-L2-4_12 in the pathogenicity of *F. proliferatum*, we performed a focused analysis using three

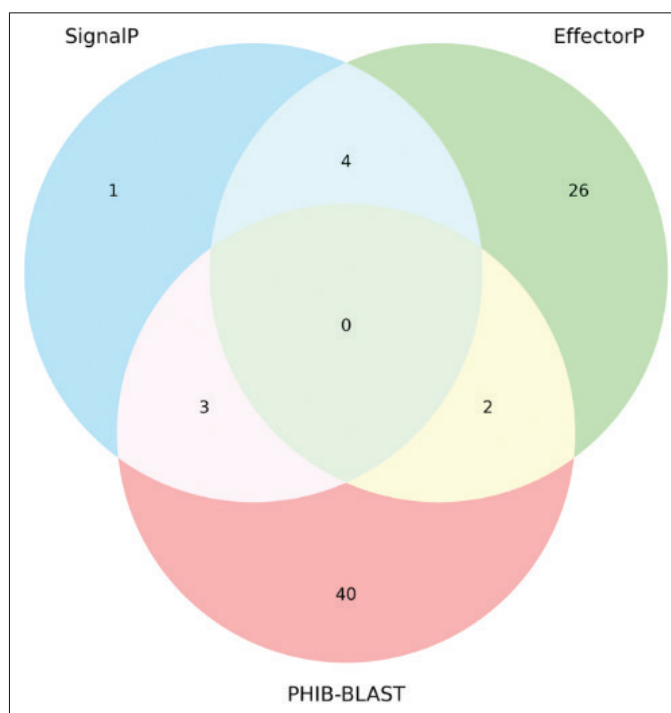


Figure 3. Venn diagram showing the overlap of predicted pathogenicity-related proteins encoded in contig ZO-L2-4_12 using three independent approaches: SignalP, and BLASTP search against the PHI-base database (E -value < 0.05). The diagram illustrates the number of proteins uniquely predicted by each tool, as well as those shared between two or all three prediction strategies.

complementary computational approaches: signal peptide prediction (SignalP), effector protein prediction (EffectorP), and homology search against a curated pathogenicity gene database (PHIB-BLAST). The overlap among predicted secreted proteins, effectors, and PHIB-BLAST is summarized in Figure 3.

SignalP was employed to identify proteins with classical N-terminal signal peptides, which are indicative of secretion through the endoplasmic reticulum-Golgi pathway [25]. Proteins secreted via this pathway often include enzymes and effectors involved in host colonization and virulence. From contig ZO-L2-4_12, a total of eight proteins were predicted to contain signal peptides, highlighting their potential role as secreted pathogenicity factors.

EffectorP was used to identify candidate effector proteins, which are proteins capable of modulating host defense responses [26]. Effector prediction is particularly important in filamentous plant pathogens, where effectors are central to host specificity and virulence. The analysis yielded 32 candidate effector proteins located on ZO-L2-4_12, supporting the hypothesis that this contig may harbor genes relevant to pathogenicity.

To further characterize the functional potential of genes encoded on ZO-L2-4_12, we performed a PHIB-BLAST (PHI-base BLAST) search, in which predicted protein sequences were queried against PHI-base (Pathogen-Host Interaction Database), a curated repository of experimentally validated pathogenicity, virulence, and effector genes from

fungal pathogens [27]. We applied *E*-value threshold of <0.05 to retain only high-confidence homologs. This analysis identified 45 proteins on ZO-L2-4_12 that exhibit significant similarity to known virulence-associated proteins, suggesting potential functional roles in host-pathogen interactions.

Collectively, the identification of secreted proteins, candidate effectors, and homologs of known pathogenicity genes on contig ZO-L2-4_12 suggests that this putative accessory chromosome may contribute to the virulence of *F. proliferatum*. Although it lacks core conserved genes, its gene content needs further investigation, particularly with respect to host specificity and adaptation.

3.5. BGCs and HRMS analysis

Secondary metabolites produced by *Fusarium* display a highly diverse chemical framework. They are usually biosynthesized by multi-domain core synthases with several additional enzymes within a biosynthetic pathway to create the final compound. These enzymes are encoded by a collective of genes that are co-regulated and located adjacent to each other, forming BGCs [28].

The AntiSMASH analysis revealed that *F. proliferatum* ZO-L2-4 has 43 BGCs spread across 11 contigs, as shown in Figure 4 and Table 4. These include seven terpene biosynthetic genes, seven nonribosomal peptide synthase (NRPS)-like, six polyketide synthases (PKS) with five type I PKS (T1PKS) and one type III PKS (T3PKS), five NRPS, four ribosomally synthesized and post-translationally modified peptides, fungal-like subtype (fungal-RiPP-like), four hybrid NRPS + T1PKS, three indole biosynthetic genes, two hybrid NRPS-like + T1PKS,

one arylpolyene, one betalactone, one isocyanide, one hybrid isocyanide-NRP + NRPS, and one hybrid NRP-metallophore + NRPS. These findings were confirmed by a previous study, which revealed that a *Fusarium* species could contain BGC numbers ranging from 39 to 57 clusters, dominated by terpene synthases, NRPS, and PKS [29,30]. Among these, only 13 BGCs showed homology with known clusters based on MIBig comparison. Only six BGCs displayed high similarity (>70%) from these, such as oxyjavanicin, choline, bikaverin, *Alternaria citri* toxin (ACT)-toxin II, koraiol, and gibepyrone-A (Table 4)

Terpene synthases are responsible for the biosynthesis of a wide array of natural terpenoid structures. NRPS encodes multi-modular enzymes that synthesize oligopeptides from amino acid monomers. A complete NRPS enzyme comprises a domain for adenylation, peptide acyl-carrier, and condensation. Each module may contain epimerization or N-methylation domains, enhancing the structural chemical diversity of non-ribosomal peptides. Meanwhile, a PKS encodes enzymes with several domains that at least consist of beta-keto synthase, acyl-transferase, and acyl-carrier protein domains, which together synthesize a polyketide chain [31]. Terpenoids, non-ribosomal peptides, and polyketides, which these BGCs generate, are the most prolific class of compounds produced by the *Fusarium* species [10,32].

The BGCs identification revealed that *F. proliferatum* ZO-L2-4 has BGCs that are responsible for the production of pigments and mycotoxins (Fig. 5). Region 2.4 had homology with T1PKS of oxyjavanicin from *Fusarium fujikuroi* (MIBiG accession BGC0001242) [33]. Region 5.2 was found to share high similarity with the bikaverin

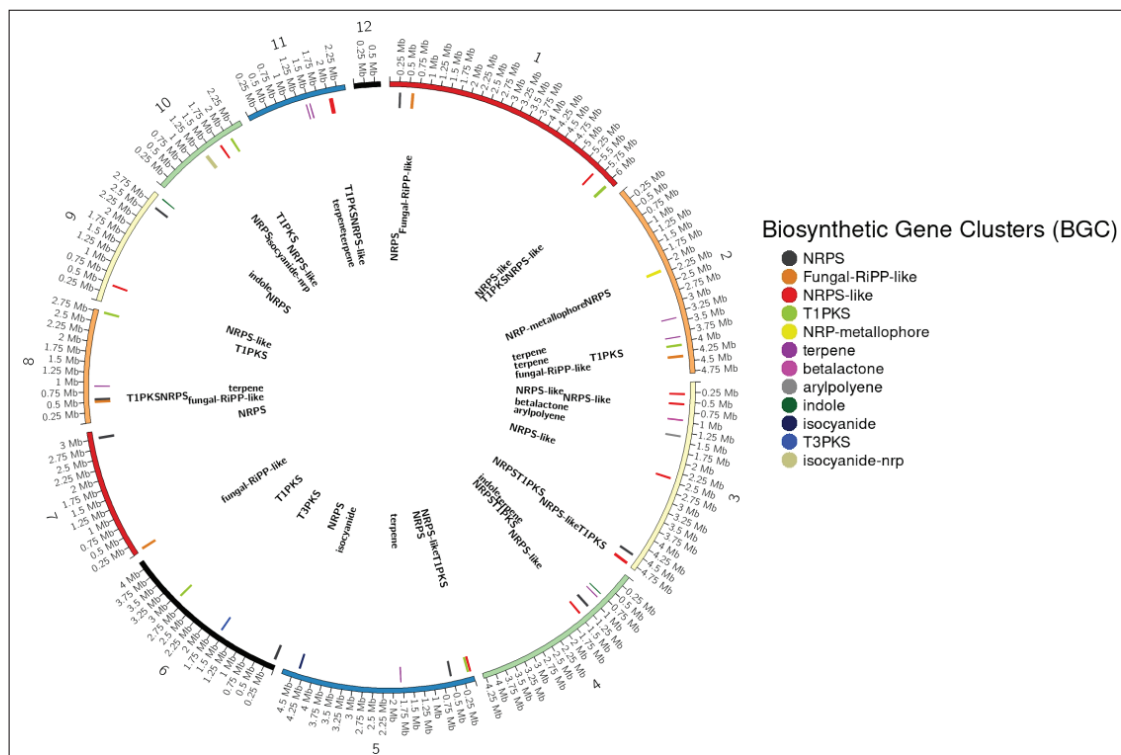


Figure 4. Circos map visualization of BGC analysis from *F. proliferatum* ZO-L2-4 genome. NRP = nonribosomal peptide.

Table 4. Identified BGCs from the *F. proliferatum* ZO-L2-4.

BGC	Type	From	To	Known clusters with the highest similarity (%)
Contig ZO-L2-4_1				
Region 1.1	NRPS	237,707	285,728	Unknown
Region 1.2	Fungal-RiPP-like	549,575	610,696	Unknown
Region 1.3	NRPS-like	5,570,792	5,614,120	Unknown
Region 1.4	NRPS-like, T1PKS	6,005,753	6,072,904	Unknown
Contig ZO-L2-4_2				
Region 2.1	NRP-metallophore, NRPS	2,138,052	2,201,906	Unknown
Region 2.2	Terpene	3,390,235	3,412,099	Aqualestatin S1 (40%)
Region 2.3	Terpene	3,868,191	3,891,488	Unknown
Region 2.4	T1PKS	4,066,290	4,113,604	Oxyjavanicin (100%)
Region 2.5	Fungal-RiPP-like	4,340,993	4,401,533	Unknown
Contig ZO-L2-4_3				
Region 3.1	NRPS-like	270,809	315,956	Unknown
Region 3.2	NRPS-like	525,045	568,899	Choline (100%)
Region 3.3	Betalactone	932,321	964,947	Unknown
Region 3.4	Arylpolyene	1,334,114	1,376,455	Unknown
Region 3.5	NRPS-like	2,408,304	2,452,221	Unknown
Region 3.6	NRPS, T1PKS	4,533,256	4,585,528	Equisetin (54%)
Region 3.7	NRPS-like, T1PKS	4,779,645	4,848,963	Fusaric acid (65%)
Contig ZO-L2-4_4				
Region 4.1	Indole	746,977	768,188	Unknown
Region 4.2	Terpene	859,873	880,598	Unknown
Region 4.3	NRPS, T1PKS	1,170,666	1,225,786	Unknown
Region 4.4	Indole	746,977	768,188	Unknown
Contig ZO-L2-4_5				
Region 5.1	NRPS-like	32,210	75,260	Fusaridione A (12%)
Region 5.2	T1PKS	90,716	139,305	Bikaverin (71%)
Region 5.3	NRPS	530,476	578,108	Unknown
Region 5.4	Terpene	1,801,366	1,822,532	Unknown
Region 5.5	Isocyanide	4,348,739	4,390,918	Unknown
Contig ZO-L2-4_6				
Region 6.1	NRPS	53,182	97,207	Acetylaranotin (30%)
Region 6.2	T3PKS	1,563,878	1,605,388	Unknown
Region 6.3	T1PKS	2,892,833	2,940,319	Unknown
Contig ZO-L2-4_7				
Region 7.1	Fungal-RiPP-like	9,404	70,894	Unknown
Region 7.2	NRPS	2,989,892	3,052,311	Unknown
Contig ZO-L2-4_8				
Region 8.1	Fungal-RiPP-like	485,275	545,807	Unknown
Region 8.2	NRPS, T1PKS	549,091	600,955	ACT-toxin II (100%)
Region 8.3	Terpene	895,270	916,162	Koraiol (100%)
Region 8.4	T1PKS	2,730,974	2,780,024	Unknown
Contig ZO-L2-4_9				
Region 9.1	NRPS-like	446,951	490,121	Unknown
Region 9.2	NRPS	2,657,370	2,706,780	Beauvericin (20%)
Region 9.3	Indole	2,950,626	2,972,870	Unknown

Continued

BGC	Type	From	To	Known clusters with the highest similarity (%)
Contig ZO-L2-4_10				
Region 10.1	Isocyanide-NRP, NRPS	1,265,414	1,355,558	Unknown
Region 10.2	NRPS-like	1,720,590	1,763,937	Unknown
Region 10.3	TIPKS	2,034,473	2,082,727	Trichoxide (41%)
Contig ZO-L2-4_11				
Region 11.1	Terpene	1,426,788	1,448,108	Unknown
Region 11.2	Terpene	1,518,355	1,540,343	Unknown
Region 11.3	NRPS, TIPKS	2,022,581	2,114,649	Gibpeyrone-A (80%)

NRP = non-ribosomal peptide.

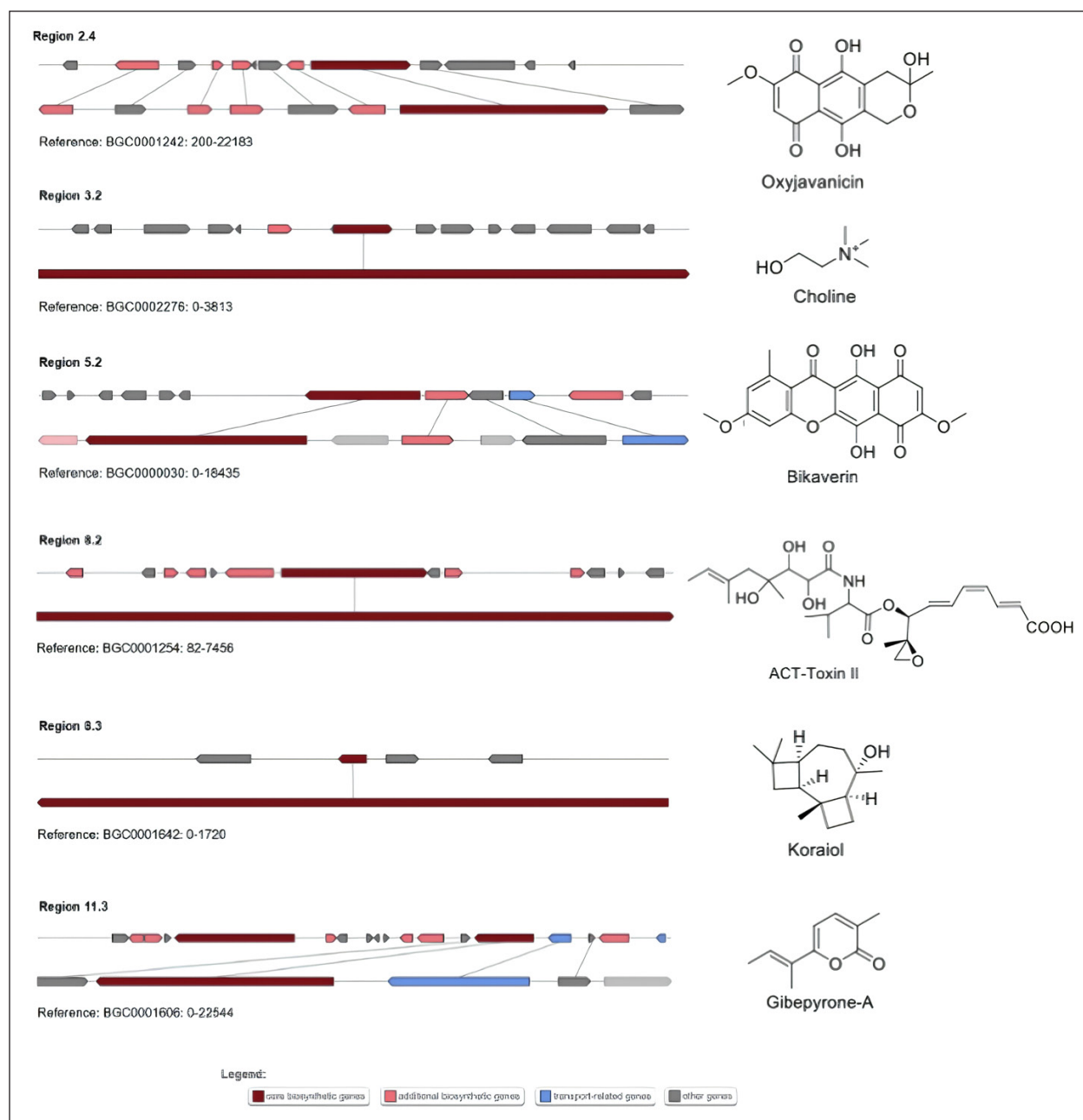
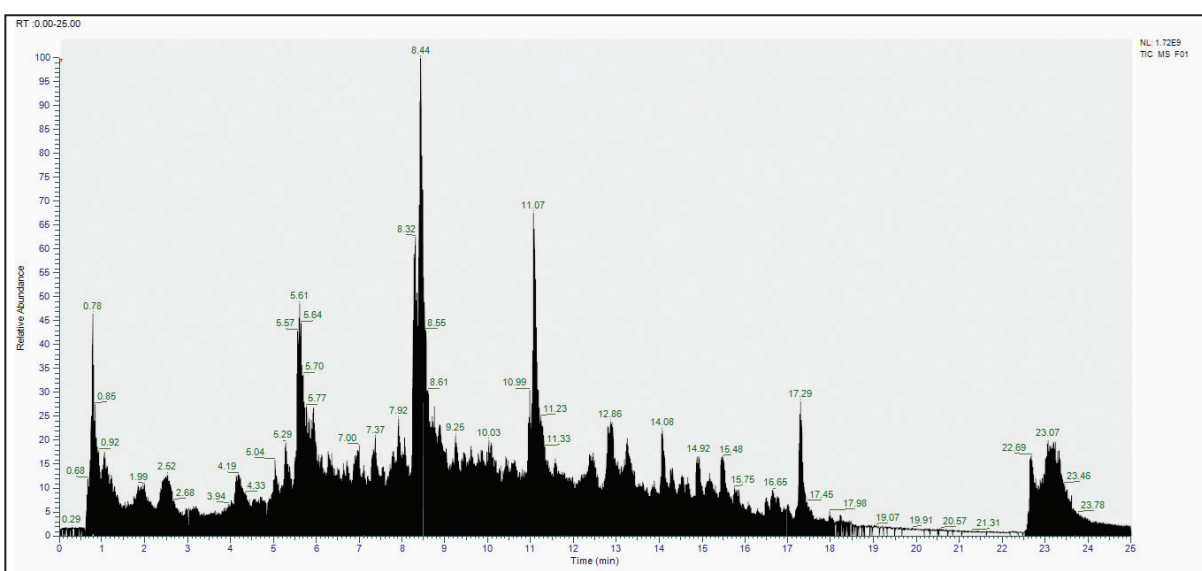


Figure 5. Comparison of the BGC components in *F. proliferatum* ZO-L2-4 with the identified BGCs responsible for the biosynthesis of oxyjavanicin, choline, bikaverin, ACT-toxin II, koraiol, and gibpeyrone-A.

Table 5. Putative metabolites identified in a *F. proliferatum* extract using untargeted HRMS analysis.

Compound Class	Putative name	Formula	Annot. DeltaMass [ppm]	Calc. MW	RT [minutes]	Area (Max.)	Ref
Alkaloids/Indole Derivatives	Tryptophol	C ₁₀ H ₁₁ N O	-0.48	161.08399	6.597	27,646,505.79	[43]
Terpenoids	Terpestacin	C ₂₅ H ₃₈ O ₄	-2.12	402.27616	10.82	2,448,498,950	[44]
Steroids	Ergosterol peroxide	C ₂₈ H ₄₄ O ₃	-2.39	428.32802	14.497	38,143,383.23	[45]
Alkaloids/Indole Derivatives	Indole	C ₈ H ₇ N	-1.45	117.05768	15.358	103,237,263.8	[46]
Nonribosomal peptide	Beauvericin	C ₄₅ H ₅₇ N ₃ O ₉	-2.82	783.40727	15.459	1,099,713,3422	[47, 48]
Alkaloids/Indole Derivatives	Terpendole E	C ₂₈ H ₃₉ N O ₃	-2.18	437.29204	16.159	18,581,919.99	[49,50]

Metabolite profiling was conducted using HRMS with Compound Discoverer 3.2, and annotations were performed via GNPS molecular networking. Compound identifications are putative, based on spectral matching and database comparisons. Based on HRMS analysis, beauvericin seems to be the predominant metabolite detected in the *F. proliferatum* ZO-L2-4 methanolic extract.

**Figure 6.** Total ion chromatogram of untargeted LC-HRMS from the methanolic extract of *F. proliferatum* ZO-L2-4.

BGC of *F. fujikuroi* (BGC0000030) [34]. Oxyjavanicin and bikaverin are polyketide pigments that have been reported to show antibacterial activities [35]. Region 3.2 showed the closest similarity to choline BGC from *Aspergillus nidulans* (BGC0002276) [36]. Choline is essential for the biosynthesis of phosphatidylcholine, a phospholipid in fungal cell membranes [37]. Region 8.2 showed similarity to ACT-toxin II BGC of *Alternaria alternata* (BGC0001254) [38], and Region 8.3 showed high similarity to BGC of koraiol from *F. fujikuroi* (BGC0001642) [39]. ACT-toxin is a compound that is highly toxic to susceptible citrus cultivars [40]. Koraiol belongs to a product of a terpene synthase/cyclase, which has been identified in various *Fusarium* accessory chromosome sequences. However, the functional role of these secondary metabolites as virulence factors of *Alternaria* and *Fusarium* hosts remains unclear [24]. AntiSMASH analysis showed that Region 11.3 has a close similarity to the BGC of gibepyrone-A

from *F. fujikuroi* (BGC0001606) [41]. This compound is a fungal toxin isolated from the rice pathogen *F. fujikuroi* [42].

Among the identified BGCs (Table 4), only beauvericin was detected in the methanolic extract of *F. proliferatum* through putative metabolite identification employing HRMS (Figs. 6 and 7, Table 5) [43–50]. The result showed that beauvericin seems to be the predominant metabolite detected in this analysis. Beauvericin is a cyclohexadepsipeptide that consists of an alternating sequence of three D-hydroxyisovaleric acids (D-Hiv) and three N-methyl-L-phenylalanine (NMe-Phe). It is synthesized through an NRPS [51]. In our findings, it is comprised of two modules, M1 and M2. M1 consists of the condensation domain, the adenylation domain, and the peptidyl carrier protein, which together load and incorporate D-Hiv to the next module, M2. M2 consists of a similar domain as M1, with the addition of an N-methyltransferase domain that methylates the amino group

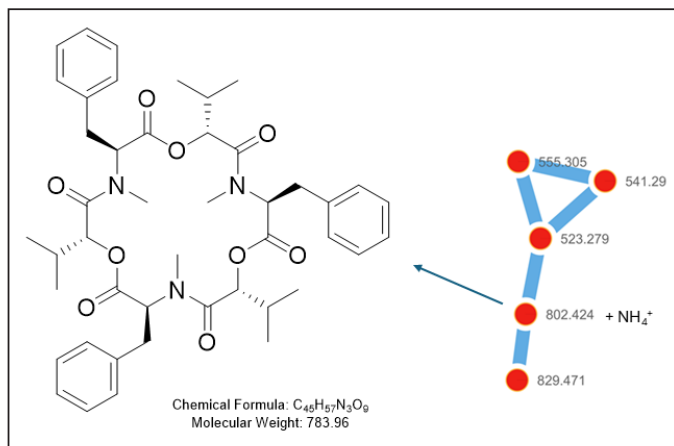


Figure 7. Putative beauvericin analogues identified via GNPS molecular networking. GNPS-based molecular networking reveals a cluster of nodes corresponding to beauvericin and structurally related analogues. The proximity and high spectral similarity of features with $[M + H]^+$ m/z 555.305, 541.290, 523.279, and 829.471 suggest the presence of unknown or uncharacterized compounds within the beauvericin molecular family.

of phenylalanine, turning it into NMe-Phe. M2 incorporates NMe-Phe to the D-Hiv. Collectively, M1 and M2 form one D-Hiv–NMe-Phe dipeptide unit in one cycle. The cycle is iterated for two more times using the generated peptides to form the six-membered-ring structure of beauvericin [51]. Despite the 20% sequence similarity with known beauvericin clusters, Region 9.2 shows domain architecture and metabolite output consistent with beauvericin biosynthesis. This suggests a divergent or strain-specific variant, possibly shaped by gene relocation or other mechanisms [52]. The compounds of the remaining BGCs were not detected in the extract. This might be because the BGCs remain silent under the fermentation conditions used in our laboratory [53].

Besides beauvericin, HRMS analysis also showed the presence of tryptophol, terpestacin, ergosterol peroxide, indole, and terpendole E (Table 5). Indole, terpendole E, and terpestacin biosynthetic genes were not detected in the BGC analysis, but they might be produced by the unidentified BGCs in this study. Indole BGC of Region 9.3 might be responsible for the production of indole that was detected in the extract. Terpendole E is an indole diterpene that is biosynthesized by the hydroxylation of paspaline by TerQ, a P450 monooxygenase protein. In *Chaunopycnis alba*, the *TerQ* gene is clustered with six other genes, including two P450 monooxygenases (*TerP* and *TerK*), an Flavin Adenine Dinucleotide (FAD)-dependent monooxygenase (*TerM*), a terpene cyclase (*TerB*), and two prenyltransferases (*TerC* and *TerF*) [54]. *TerF* and *TerP* from *C. alba* (BGC0001260.3) exhibited homology with two sequences in the indole BGC of Region 4.1 in this study, and the detected terpendole E in this study might be produced via this BGC. Meanwhile, terpestacin is a sesterterpene that is synthesized via terpene synthase BGC. In *F. proliferatum* NRRL62905, this BGC comprises four genes, including *tpcB*, *tpcA*, *tpcD*, and *tpcC*, which respectively encode P450-1, terpene cyclase, flavin-dependent oxidase, and P450-2 [55]. AntiSMASH analysis showed that Region 2.3 and 11.1 consist of P450

and terpene synthase genes, which might be involved in the terpestacin biosynthesis. As we employed short-read sequencing in this study, the undetected BGCs for indole, terpendole E, and terpestacin might be fragmented and separated by gaps in the assembly, resulting in the detection of incomplete BGCs [56,57].

Tryptophol and ergosterol peroxide were not detected in the BGC analysis because their biosynthesis does not involve a canonical BGC. Instead, they are formed through primary metabolic pathways or simple enzymatic conversions outside canonical BGC. Tryptophol is derived from L-tryptophan via the tryptophan-dependent enzymatic [43]. Meanwhile, ergosterol peroxide is a steroid that is biosynthesized by oxidative modification of ergosterol [58].

In our previous study [11], a pyridine-containing polyketide, 8-*O*-methylbostrycoidin was tentatively identified by LC-MS/MS analysis from the methanolic extract of *F. proliferatum* ZO-L2-4, however, it was not detected in the current HRMS analysis. We assumed that the production of this compound may be suppressed following repeated fungal fermentation. Therefore, further study on isolation and structure elucidation of secondary metabolites produced by this fungus would be needed to verify the result from BGCs analysis in combination with the metabolite profile from HRMS analysis afforded in the present study.

Our previous study also reported that the methanolic extract of *F. proliferatum* ZO-L2-4 showed promising antibacterial and cytotoxicity [11]. The detected compounds in the extract might contribute to the reported bioactivities. For instance, beauvericin was previously reported to have antimicrobial activity against *Candida albicans*, *Escherichia coli*, and *Staphylococcus aureus*, with the strongest effect observed against *S. aureus* (the Minimum Inhibition Concentration/MIC = 3.91 μ M), which is comparable to the activity of amoxicillin as a positive control [59]. Indole alkaloids isolated from the endophytic fungus *Robillarda sessilis* demonstrated moderate antibacterial activity against Methicillin-Resistant *Staphylococcus aureus* (MRSA) (MIC = 12.5 μ g/ml) [60], while ethyl 3-indoleacetate from *F. proliferatum* T2-10 exhibited anticancer potential as a horseradish peroxidase-activated prodrug [61,62]. Terpestacin was shown to possess antibacterial activities against *Mycobacterium marinum* ATCCBAA-535 with an IC_{50} of 84 μ M [63]. Ergosterol peroxide was found to have antibacterial activity by disrupting the electron transport chain and oxidative phosphorylation in the bacterial membrane cells [64]. Terpendole E was reported to have potential as a specific inhibitor of Eg5 myosin protein in the development of antitumor drugs [65].

Unlike previously sequenced *F. proliferatum* strains, our isolate originated from ginger rhizomes. Endophytic origin of fungi could offer a more diverse BGCs compared to their counterparts that are isolated from a non-endophytic source [66]. Thus, the high proportion of the unknown BGCs in our study indicates an untapped biosynthetic potential of this strain, making it a valuable source for further genome mining and activation studies for drug discovery.

4. CONCLUSION

The Anti-SMASH analysis revealed that *F. proliferatum* ZO-L2-4 has 43 BGCs for secondary metabolites, comprising seven terpene biosynthetic genes, seven NRPS-like, six PKS (five T1PKS and one T3PKS), five NRPS, four fungal-RiPP-like, four hybrid NRPS + T1PKS, three indole biosynthetic genes, two hybrid NRPS-like + T1PKS, one arylpolyene, one betalactone, one isocyanide, one hybrid isocyanide-NRP + NRPS, and one hybrid NRP-metallophore + NRPS. Among these, only 13 BGCs showed the highest similarity with known clusters based on MIBig comparison. Out of these, only six BGCs displayed high similarity. This was confirmed by HRMS analysis, which detected beauvericin and other metabolites in the methanolic extract of the fungus. However, the remaining BGCs are considered unknown by far. These findings create opportunities for targeted genome mining techniques, including gene knockout or heterologous expression to activate silent BGCs and produce novel bioactive secondary metabolites for drug discovery and development.

5. ACKNOWLEDGMENT

Financial support from The Directorate General of Higher Education, Ministry of Education, Culture, Research and Technology, Republic of Indonesia, through Fundamental Research Program 2024, grant number: B/519-39/UN.14.4.A/PT.01.03/2024, is gratefully acknowledged. The authors also acknowledge the facilities, scientific and technical support from National Research and Innovation Agency (BRIN), Gunungkidul, through E-Layanan Sains (ELSA) BRIN.

6. AUTHORS CONTRIBUTION

All authors made substantial contributions to conception and design, acquisition of data, or analysis and interpretation of data; took part in drafting the article or revising it critically for important intellectual content; agreed to submit to the current journal; gave final approval of the version to be published; and agree to be accountable for all aspects of the work. All the authors are eligible to be an author as per the International Committee of Medical Journal Editors (ICMJE) requirements/guidelines.

7. CONFLICTS OF INTEREST

The authors report no financial or any other conflicts of interest in this work.

8. ETHICAL APPROVALS

This study does not involve experiments on animals or human subjects.

9. DATA AVAILABILITY

All the data is available with the authors and shall be provided upon request.

10. PUBLISHER'S NOTE

All claims expressed in this article are solely those of the authors and do not necessarily represent those of the publisher, the editors and the reviewers. This journal remains

neutral with regard to jurisdictional claims in published institutional affiliation.

11. USE OF ARTIFICIAL INTELLIGENCE (AI)-ASSISTED TECHNOLOGY

The authors declare that they have not used artificial intelligence (AI)-tools for writing and editing of the manuscript, and no images were manipulated using AI.

12. SUPPLEMENTARY MATERIAL

The supplementary material can be accessed at the Link here: https://japsonline.com/admin/php/uploadss/4766_pdf.pdf

REFERENCES

- Zakariyah RF, Ajijolakewu KA, Ayodele AJ, Folami-A BI, Samuel EP, Otuoze SO, *et al.* Progress in endophytic fungi secondary metabolites: biosynthetic gene cluster reactivation and advances in metabolomics. *Bull Natl Res Cent.* 2024 48(44):1–18. doi: <https://doi.org/10.1186/s42269-024-01199-x>
- Sagita R, Quax WJ, Haslinger K. Current state and future directions of genetics and genomics of endophytic fungi for bioprospecting efforts. *Front Bioeng Biotechnol.* 2021;9:649906. doi: <https://doi.org/10.3389/fbioe.2021.649906>
- Hong L, Wang Q, Zhang J, Chen X, Liu Y, Asiegbu FO, *et al.* Advances in the beneficial endophytic fungi for the growth and health of woody plants. *For Res (Fayettev).* 2024;4:28. doi: <https://doi.org/10.48130/forres-0024-0025>
- Waqar S, Bhat AA, Khan AA. Endophytic fungi: unravelling plant-endophyte interaction and the multifaceted role of fungal endophytes in stress amelioration. *Plant Physiol Biochem.* 2024;206:108174. doi: <https://doi.org/10.1016/j.plaphy.2023.108174>
- Akram S, Ahmed A, He P, He P, Liu Y, Wu Y, *et al.* Uniting the role of endophytic fungi against plant pathogens and their interaction. *J Fungi (Basel).* 2023;9(1):72. doi: <https://doi.org/10.3390/jof9010072>
- Enyi EO, Chigozie VU, Okezie UM, Udeagbala NT, Oko AO. A review of the pharmaceutical applications of endophytic fungal secondary metabolites. *Nat Prod Res.* 2025. 39(11):3295-3311. doi: <https://doi.org/10.1080/14786419.2024.2423036>
- Singh VK, Kumar A. Secondary metabolites from endophytic fungi: production, methods of analysis, and diverse pharmaceutical potential. *Symbiosis.* 2023;90:111–25. doi: <https://doi.org/10.1007/s13199-023-00925-9>
- Toghueo RMK. Bioprospecting endophytic fungi from *Fusarium* genus as sources of bioactive metabolites. *Mycology.* 2019;11(1):1–21. doi: <https://doi.org/10.1080/21501203.2019.1645053>
- Li M, Yu R, Bai X, Wang H, Zhang H. *Fusarium*: a treasure trove of bioactive secondary metabolites. *Nat Prod Rep.* 2020;37:1568–88. doi: <https://doi.org/10.1039/D0NP00038H>
- Amuzu P, Pan X, Hou X, Sun J, Jakada MA, Odigie E, *et al.* Recent updates on the secondary metabolites from *Fusarium* fungi and their biological activities (Covering 2019 to 2024). *J Fungi (Basel).* 2024;10(11):778. doi: <https://doi.org/10.3390/jof10110778>
- Ariantari NP, Putra IPYA, Dwiyaning NMW, Leliqia NPE, Wirajana IN, Yustiantara PS, *et al.* Antimicrobial, cytotoxicity, and LC-MS/MS analysis of methanolic extract of *Fusarium proliferatum* ZO-L2-4, an endophytic fungus isolated from *Zingiber officinale* Roscoe. *J Pharm Pharmacogn Res.* 2025;13(1):152–62. doi: https://doi.org/10.56499/jppres23.1899_13.1.152
- Ma RH, Ni ZJ, Zhu YY, Thakur K, Zhang F, Zhang YY, *et al.* A recent update on the multifaceted health benefits associated with ginger and its bioactive components. *Food Funct.* 2021;12:519–42. doi: <https://doi.org/10.1039/D0FO02834G>

13. Zhang M, Zhao R, Wang D, Wang L, Zhang Q, Wei S, *et al.* Ginger (*Zingiber officinale* Rosc.) and its bioactive components are potential resources for health beneficial agents. *Phytotherapy Res.* 2021;35(2):711–42. doi: <https://doi.org/10.1002/ptr.6858>
14. Hardi H, Estuworo GK, Louisa M. Effectivity of oral ginger supplementation for chemotherapy induced nausea and vomiting (CINV) in children: a systematic review of clinical trials. *J Ayurveda Integr Med.* 2024;15(4):100957. doi: <https://doi.org/10.1016/j.jaim.2024.100957>
15. Ayustaningwarno F, Anjani G, Ayu AM, Fogliano V. A critical review of Ginger's (*Zingiber officinale*) antioxidant, anti-inflammatory, and immunomodulatory activities. *Front Nutr.* 2024;11:1364836. doi: <https://doi.org/10.3389/fnut.2024.1364836>
16. Choi JG, Kim SY, Jeong M, Oh MS. Pharmacotherapeutic potential of ginger and its compounds in age-related neurological disorders. *Pharmacol Ther.* 2018;182:56–69. doi: <https://doi.org/10.1016/j.pharmthera.2017.08.010>
17. Ariantari NP, Ancheeva E, Wang C, Mándi A, Knedel TO, Kurtán T, *et al.* Indole diterpenoids from an endophytic *Penicillium* sp. *J Nat Prod.* 2019;82(6):1412–23. doi: <https://doi.org/10.1021/acs.jnatprod.8b00723>
18. Harwoko H, Lee J, Daletos G, Feldbrügge M, Kalscheuer R, Prosch P. Antimicrobial compound from *Trichoderma harzianum*, an endophytic fungus associated with ginger (*Zingiber officinale*). *J. Kedokt. Kesehat. Indones.* 2021;12(2):151–7. doi: <https://doi.org/10.20885/JKKI.Vol12.Iss2.art8>
19. Dame ZT, Silima B, Gryzenhout M, Van Ree T. Bioactive compounds from the endophytic fungus *Fusarium proliferatum*. *Nat Prod Res.* 2016;30(11):1301–4. doi: <https://doi.org/10.1080/14786419.2015.1053089>
20. Li T, Yang W, Chen T, Ouyang H, Liu Y, Wang B, *et al.* Five secondary metabolites from mangrove endophytic fungus *Fusarium proliferatum* NSD-1. *J Mol Struct.* 2024;1302:137434. doi: <https://doi.org/10.1016/j.molstruc.2023.137434>
21. Kjærboelling I, Mortensen UH, Vesth T, Andersen MR. Strategies to establish the link between biosynthetic gene clusters and secondary metabolites. *Fungal Genet Biol.* 2019;130:107–21. doi: <https://doi.org/10.1016/j.fgb.2019.06.001>
22. Li L. Next-generation synthetic biology approaches for the accelerated discovery of microbial natural products. *Eng Microbiol.* 2023;3(1):100060. doi: <https://doi.org/10.1016/j.engmic.2022.100060>
23. Cano-Prieto C, Undabarrena A, De Carvalho AC, Keasling JD, Cruz-Morales P. Triumphs and challenges of natural product discovery in the postgenomic era. *Annu Rev Biochem.* 2024;93:411–45. doi: <https://doi.org/10.1146/annurev-biochem-032620-104731>
24. Witte TE, Villeneuve N, Boddy CN, Overy DP. Accessory chromosome-acquired secondary metabolism in plant pathogenic fungi: the evolution of biotrophs into host-specific pathogens. *Front Microbiol.* 2021;12:664276. doi: <https://doi.org/10.3389/fmicb.2021.664276>
25. Teufel F, Almagro Armenteros JJ, Johansen AR, Gíslason MH, Pihl SI, Tsigiris KD, *et al.* SignalP 6.0 predicts all five types of signal peptides using protein language models. *Nat Biotechnol.* 2022;40(7):1023–5. doi: <https://doi.org/10.1038/s41587-021-01156-3>
26. Sperschneider J, Dodds PN. EffectorP 3.0: prediction of apoplastic and cytoplasmic effectors in fungi and oomycetes. *Mol Plant Microbe Interact.* doi: <https://doi.org/10.1094/MPMI-08-21-0201-R>
27. Urban M, Cuzick A, Seager J, Wood V, Rutherford K, Venkatesh SY, *et al.* PHI-base: the pathogen-host interactions database. *Nucleic Acids Res.* 2020;48(D1):D613–20. doi: <https://doi.org/10.1093/nar/gkz904>
28. Nielsen MR, Sondergaard TE, Giese H, Sørensen JL. Advances in linking polyketides and non-ribosomal peptides to their biosynthetic gene clusters in *Fusarium*. *Curr Genet.* 2019;65(6):1263–80. doi: <https://doi.org/10.1007/s00294-019-00998-4>
29. Hoogendoorn K, Barra L, Waalwijk C, Dickschat JS, van der Lee TAJ, Medema MH. Evolution and diversity of biosynthetic gene clusters in *Fusarium*. *Front Microbiol.* 2018;9:1158. doi: <https://doi.org/10.3389/fmicb.2018.01158>
30. Pokhrel A, Coleman JJ. Inventory of the secondary metabolite biosynthetic potential of members within the terminal clade of the *Fusarium solani* species complex. *J Fungi.* 2023;9:799. doi: <https://doi.org/10.3390/jof9080799>
31. Zhgun AA. Fungal BGCs for production of secondary metabolites: main types, central roles in strain improvement, and regulation according to the piano principle. *Int J Mol Sci.* 2023;24(13):11184. doi: <https://doi.org/10.3390/ijms241311184>
32. Ahmed AM, Mahmoud BK, Millán-Aguinaga N, Abdelmohsen UR, Fouad MA. The endophytic *Fusarium* strains: a treasure trove of natural products. *RSC Adv.* 2023;13(2):1339–69. doi: <https://doi.org/10.1039/D2RA04126J>
33. Studt L, Wiemann P, Kleigrew K, Humpf HU, Tudzynski B. Biosynthesis of fusarubins accounts for pigmentation of *Fusarium fujikuroi* perithecia. *Appl Environ Microb.* 2012;78(12):4468–80. doi: <https://doi.org/10.1128/aem.00823-12>
34. Son SW, Kim HY, Choi GJ, Lim HK, Jang KS, Lee SO, *et al.* Bikaverin and fusaric acid from *Fusarium oxysporum* show antioomycete activity against *Phytophthora infestans*. *J Appl Microbiol.* 2008;104(3):692–8. doi: <https://doi.org/10.1111/j.1365-2672.2007.03581.x>
35. Studt L, Tudzynski B. Gibberellins and the Red Pigments Bikaverin and Fusarubin. In: Martin, JF., García-Estrada, C., Zeilinger, S. (eds) *Biosynthesis and Molecular Genetics of Fungal Secondary Metabolites*. Fungal Biology. Springer, New York, USA. 2014: 209–38. doi: https://doi.org/10.1007/978-1-4939-1191-2_10
36. Hai Y, Huang AM, Tang Y. Structure-guided function discovery of an NRPS-like glycine betaine reductase for choline biosynthesis in fungi. *Proc Natl Acad Sci U S A.* 2019;116(21):10348–53. doi: <https://doi.org/10.1073/pnas.1903282116>
37. Markham P, Robson GD, Bainbridge BW, Trinci AP. Choline: its role in the growth of filamentous fungi and the regulation of mycelial morphology. *FEMS Microbiol Rev.* 1993;10(3-4):287–300. doi: <https://doi.org/10.1111/j.1574-6968.1993.tb05872.x>
38. Miyamoto Y, Masunaka A, Tsuge T, Yamamoto M, Ohtani K, Fukumoto T, *et al.* ACTTS3 encoding a polyketide synthase is essential for the biosynthesis of ACT-toxin and pathogenicity in the tangerine pathotype of *Alternaria alternata*. *Mol Plant Microbe Interact.* 2010;23(4):406–14. doi: <https://doi.org/10.1094/mpmi-23-4-0406>
39. Brock NL, Huss K, Tudzynski B, Dickschat JS. Genetic dissection of sesquiterpene biosynthesis by *Fusarium fujikuroi*. *Chembiochem.* 2013;14(3):311–5. doi: <https://doi.org/10.1002/cbic.201200695>
40. Chen Y, Cao Y, Jiao C, Sun X, Gai Y, Zhu Z, *et al.* The *Alternaria alternata* StuA transcription factor interacting with the pH-responsive regulator PacC for the biosynthesis of host-selective toxin and virulence in citrus. *Microbiol Spectr.* 2023;11(6):233523 <https://doi.org/10.1128/spectrum.02335-23>
41. Janevska S, Arndt B, Niehaus EM, Burkhardt I, Rösler SM, Brock NL, *et al.* Gibberone biosynthesis in the rice pathogen *Fusarium fujikuroi* is facilitated by a small polyketide synthase gene cluster. *J Biol Chem.* 2016;291(53):27403–20. doi: <https://doi.org/10.1074/jbc.m116.753053>
42. Lin C, Feng XL, Liu Y, Li ZC, Li XZ, Qi J. Bioinformatic analysis of secondary metabolite biosynthetic potential in pathogenic *Fusarium*. *J Fungi.* 2023;9(8):850. doi: <https://doi.org/10.3390/jof9080850>
43. Luo K, Desroches CL, Johnston A, Harris LJ, Zhao HY, Ouellet T. Multiple metabolic pathways for metabolism of L-tryptophan in *Fusarium graminearum*. *Can J Microbiol.* 2017;63(11):921–7. doi: <https://doi.org/10.1139/cjm-2017-0383>
44. Sun X, Li Y, Xu H, Huang S, Liu Y, Liao S, *et al.* Terpestacin and its derivatives: bioactivities and syntheses. *Chem Biodivers.* 2025;22(1):202401905. doi: <https://doi.org/10.1002/cbdv.202401905>

45. Han S, Sheng B, Zhu D, Chen J, Cai H, Zhang S, *et al.* Role of FoERG3 in ergosterol biosynthesis by *Fusarium oxysporum* and the associated regulation by *Bacillus subtilis* HSY21. *Plant Dis.* 2023;107(5):1565–75. doi: <https://doi.org/10.1094/pdis-05-22-1010-re>
46. Luo K, Rocheleau H, Qi PF, Zheng YL, Zhao HY, Ouellet T. Indole-3-acetic acid in *Fusarium graminearum*: identification of biosynthetic pathways and characterization of physiological effects. *Fungal Biol.* 2016;120(9):1135–45. doi: <https://doi.org/10.1016/j.funbio.2016.06.002>
47. Rana S, Singh SK, Dufossé L. Multigene phylogeny, beauvericin production and bioactive potential of *Fusarium* strains isolated in India. *J Fungi (Basel).* 2022;8(7):662. doi: <https://doi.org/10.3390/jof8070662>
48. Suhajda A, Al-Nussairawi M, Amara I, Sörös C, Tömösközi-Farkas R, Kriszt B, *et al.* Co-Occurrence of beauvericin and fumonisin producing ability of *Fusarium* strains isolated from crop plants in Hungary. *Curr Microbiol.* 2025;82(7):1–3. doi: <https://doi.org/10.1007/s00284-025-04243-9>
49. Motoyama T, Osada H. Biosynthetic approaches to creating bioactive fungal metabolites: pathway engineering and activation of secondary metabolism. *Bioorg Med Chem Lett.* 2016;26(24):5843–50. doi: <https://doi.org/10.1016/j.bmcl.2016.11.013>
50. Parker E, J, Scott D, B. Indole-diterpene biosynthesis in ascomycetous fungi. In: An, Z. (ed) *Handbook of industrial mycology.* CRC Press, Boca Raton, FL. 2004: 424– 45. doi: <https://doi.org/10.1201/9780203970553>
51. Zhang T, Zhuo Y, Jia X, Liu J, Gao H, Song F, *et al.* Cloning and characterization of the gene cluster required for beauvericin biosynthesis in *Fusarium proliferatum*. *Sci China Life Sci.* 2013;56(7):628–37. doi: <https://doi.org/10.1007/s11427-013-4505-1>
52. Proctor RH, McCormick SP, Alexander NJ, Desjardins AE. Evidence that a secondary metabolic biosynthetic gene cluster has grown by gene relocation during evolution of the filamentous fungus *Fusarium*. *Mol Microbiol.* 2009;74(5):1128–42. doi: <https://doi.org/10.1111/j.1365-2958.2009.06927.x>
53. Hoskisson PA, Seipke RF. Cryptic or silent? The known unknowns, unknown knowns, and unknown unknowns of secondary metabolism. *mBio.* 2020;11(5):2642. doi: <https://doi.org/10.1128/mbio.02642-20>
54. Motoyama T, Hayashi T, Hirota H, Ueki M, Osada H. Terpendole E, a kinesin Eg5 inhibitor, is a key biosynthetic intermediate of indole-diterpenes in the producing fungus *Chaunopycnis alba*. *Chem Biol.* 2012;19(12):1611–9. doi: <https://doi.org/10.1016/j.chembiol.2012.10.010>
55. Narita K, Minami A, Ozaki T, Liu C, Kodama M, Oikawa H. Total biosynthesis of antiangiogenic agent (–)-terpestacin by artificial reconstitution of the biosynthetic machinery in *Aspergillus oryzae*. *J Org Chem.* 2018;83(13):7042–8. doi: <https://doi.org/10.1021/acs.joc.7b03220>
56. Blin K, Shaw S, Medema MH, Weber T. The antiSMASH database version 4: additional genomes and BGCs, new sequence-based searches and more. *Nucleic Acids Res.* 2024;52(1):D586–9. doi: <https://doi.org/10.1093/nar/gkad984>
57. Sánchez-Navarro R, Nuhamunada M, Mohite OS, Wasmund K, Albertsen M, Gram L, *et al.* Long-read metagenome-assembled genomes improve identification of novel complete biosynthetic gene clusters in a complex microbial activated sludge ecosystem. *mSystems.* 2022;7(6):63222. doi: <https://doi.org/10.1128/mSystems.00632-22>
58. Merdivan S, Lindequist U. Ergosterol peroxide: a mushroom-derived compound with promising biological activities a review. *Int J Med Mushrooms.* 2017;19(2):93–105. doi: <https://doi.org/10.1615/intjmedmushrooms.v19.i2.10>
59. Zhang H, Ruan C, Bai X, Zhang M, Zhu S, Jiang Y. Isolation and identification of the antimicrobial agent beauvericin from the endophytic *Fusarium oxysporum* 5-19 with NMR and ESI-MS/MS. *Biomed Res Int.* 2016;2016:1084670. doi: <https://doi.org/10.1155/2016/1084670>
60. Huang Z, Wu D, Liu X, Liu Q, Han X, Wang W, *et al.* Indole alkaloids from endophytic fungus *Robillarda sessilis* and their antibacterial activity. *Nat Prod Res.* 2025;39(5):1156–65. doi: <https://doi.org/10.1080/14786419.2023.2297853>
61. Tan JB, Peng WW, Li MF, Kang FH, Zheng YT, Xu L, *et al.* Three new metabolites from the endophyte *Fusarium proliferatum* T2-10. *Nat Prod Res.* 2025;39(7):1793–803. doi: <https://doi.org/10.1080/14786419.2023.2278158>
62. Li H, Chen L, Shi Y, Yuan B, Ma Y, Wei H, *et al.* Design of block copolymer micellar aggregates for co-delivery of enzyme and anticancer prodrug. *Chem Asian J.* 2017;12(2):176–80. doi: <https://doi.org/10.1002/asia.201601198>
63. Deng Z, Li C, Luo D, Teng P, Guo Z, Tu X, *et al.* A new cinnamic acid derivative from plant-derived endophytic fungus *Pyronema* sp. *Nat Prod Res.* 2017;31(20):2413–19. doi: <https://doi.org/10.1080/14786419.2017.1311890>
64. Rangsinth P, Sharika R, Pattarachotanant N, Duangjan C, Wongwan C, Sillapachaiyaporn C, *et al.* Potential beneficial effects and pharmacological properties of ergosterol, a common bioactive compound in edible mushrooms. *Foods.* 2023;12(13):2529. doi: <https://doi.org/10.3390/foods12132529>
65. Reddy P, Guthridge K, Vassiliadis S, Hemsworth J, Hettiarachchige I, Spangenberg G, *et al.* Tremorgenic mycotoxins: structure diversity and biological activity. *Toxins (Basel).* 2019;11(5):302. doi: <https://doi.org/10.3390/toxins11050302>
66. Scott K, Konkel Z, Gluck-Thaler E, Valero David GE, Simmt CF, Grootmyers D, *et al.* Endophyte genomes support greater metabolic gene cluster diversity compared with non-endophytes in *Trichoderma*. *PLoS One.* 2023;18(12):289280. doi: <https://doi.org/10.1371/journal.pone.0289280>

How to cite this article:

Ariantari NP, Putra IPYA, Wiprayoga IPP, Frediansyah A, Putri NWPS, Suari AAIP, Dewi KTN, Astuti KW, Pharmawati M. Draft genome sequence of endophytic fungus *Fusarium proliferatum* ZO-L2-4 and analysis of its secondary metabolite biosynthetic potential. *J Appl Pharm Sci.* 2026;16(04):275-287. DOI: 10.7324/JAPS.2026.234783